Proceedings of the Combustion Institute 42 (2026) 106648

Contents lists available at ScienceDirect

Proceedings of the Combustion Institute

journal homepage: www.elsevier.com/locate/proci

Influence of H_2 addition on emission characteristics of SAF/Jet A1 blend in a low-swirl combustor

Francesca Picca [a,*,1], Samarjeet Singh [b,*,1], Fabio Sasso [a], Emanuele A. Scelzo [a], Mario Commodo [c], Fabian P. Hagen [b], Stefan R. Harth [b], Dimosthenis Trimis [b], Andrea D'Anna [a], Henning Bockhorn [b]

[a] Dipartimento di Ingegneria Chimica, dei Materiali e della Produzione Industriale, Università degli Studi di Napoli Federico II, Napoli, 80125, Italy
[b] Engler-Bunte-Institute, Division of Combustion Technology, Karlsruhe Institute of Technology, Karlsruhe, 76131, Germany
[c] Istituto di Scienze e Tecnologie per l'Energia e la Mobilità Sostenibili, CNR, Napoli, Italy

ARTICLE INFO

Keywords:
Hydrogen combustion
Sustainable aviation fuel
Particulate
Fuel-flexible combustor
Low-NO_x

ABSTRACT

Aviation kerosene is the primary fuel for modern aviation turbine engines. The aviation sector contributes roughly 2.4% of global CO_2 emissions and, in response, alternative fuels have been actively explored. Sustainable Aviation Fuels (SAFs), typically derived from biomasses and other renewable feedstocks, have attracted considerable attention. Under current regulations, SAFs can be blended with conventional kerosene up to 50% by volume. Moreover, SAF can reduce life-cycle greenhouse-gas emissions by up to ~89% respect to conventional kerosene. Hydrogen (H_2) represents another promising alternative, as it burns without carbon emissions and has a higher mass-based energy content compared to hydrocarbon fuels. Blending SAF (or conventional jet fuel) with H_2 is being considered as a transitional pathway towards a more sustainable aviation. However, successful adoption of such blends requires a detailed understanding of their combustion characteristics. In this study, we investigate the flame stabilization and pollutant emissions in an innovative fuel-flexible combustor operating with Jet A1, HEFA-SAF (i.e., SAF produced from Hydroprocessed Esters and Fatty Acids), and H_2 at atmospheric pressure and elevated air inlet temperatures. Significant attention is directed toward particulate (soot) emissions from the flames fuelled with HEFA-SAF/Jet A1 blends, both with and without H_2. The results reveal significant differences: small additions of H_2 can transiently increase the formation of early particulate precursors, whereas higher H_2 blends strongly suppress particulate nucleation and growth. Flames with high H_2 content achieved near-zero soot emissions and lower CO emissions, demonstrating the potential of H_2 and blended SAF/Jet A1 combustion for clean aviation propulsion.

Novelty and significance statement: The current study investigates the spatially resolved characterization of soot particle formation in an innovative fuel-flexible burner. The burner integrates a lean-lifted spray SAF/Jet A1 flame with hydrogen (H_2) injectors arranged around the prefilmer. The results demonstrate significant trends: even small H_2 additions can transiently enhance the formation of early soot precursors, while higher H_2 fractions strongly suppress soot nucleation and growth. Overall, the system maintains very low particulate emissions across the investigated conditions. These experiments provide new insights into the drop-in compatibility of dual-fuel systems, offering a viable pathway to decarbonize aviation combustion systems.

1. Introduction

Jet A1, a kerosene-based aviation fuel produced to international standards, is the primary fuel for commercial turbine aircraft worldwide due to its high energy density, safety, and infrastructure compatibility. However, Jet A1 combustion contributes to about 2.4% of global CO_2 emissions [1], motivating efforts towards low-carbon alternatives to meet aviation's 2050 net-zero goals. Among these alternatives, Sustainable Aviation Fuels (SAFs) have emerged as the most viable near-term solution for reducing carbon footprint [2]. Derived from

* Corresponding authors.
E-mail addresses: francesca.picca@unina.it (F. Picca), samarjeet.singh@kit.edu (S. Singh).
[1] These authors contributed equally to this work.

https://doi.org/10.1016/j.proci.2026.106648
Received 15 March 2026; Accepted 16 June 2026
Available online 3 November 2026
1540-7489/© 2026 The Author(s). Published by Elsevier Inc. on behalf of The Combustion Institute. This is an open access article under the CC BY license (http://creativecommons.org/licenses/by/4.0/).

renewable or waste resources, SAF is fully compatible with existing engines and infrastructure [3] and can cut life-cycle CO_2 emissions by up to ~89% compared to Jet A1 [4]. Certified under ASTM D7566, SAF can be blended up to 50% with Jet A1, but global production remains limited, highlighting the need for further research on its combustion performance and scalability.

In parallel, hydrogen (H_2) has gained increasing attention as a potential ultra-clean aviation fuel [5], offering approximately 2.5 times the energy per unit mass of kerosene [6] while reducing carbon-based emissions. The influence of H_2 on NO_x emissions is instead less straightforward. Since the increase flame speed and related flame position/shape as well as higher (local) flame temperatures may enhance NO_x formation, researchers are proposing alternative combustor designs and configurations to mitigate NO_x emissions [7–9]. In addition, challenges related to the low volumetric energy density of hydrogen, as well as fuel storage and infrastructure requirements, still slow down large-scale adoption [10]. H_2-enriched or dual-fuel systems offer a bridge to low-carbon aviation, using H_2 in current engines with minimal changes [11]. These new burner designs aim to improve mixing, prevent flashback, and reduce NO_x emissions. Building on these advances, several studies have explored dual-fuel combustion, systematically exploring partial or full range of hydrogen blending with conventional kerosene, under realistic engine conditions and across different combustor configurations [12–18].

While most of this research has primarily focused on flame stability and NO_x emissions, less attention has been devoted to particulate emissions and soot formation. Early research by Hiroyasu et al. [12] showed how different H_2 blending ratios affect flame stability, efficiency, and emissions in a gas turbine combustor, including soot formation. They reported that the highest soot concentration occurred for a flame with a hydrogen blending ratio of 10%. Dave et al. [13] investigated the macroscopic behavior of kerosene–H_2 blended flames in a multi-fuel combustor, inferring sooting tendencies from changes in flame topology, luminosity, and color with increasing hydrogen fraction. In a recent work, Mohammadnejad et al. [18] investigated the influence of hydrogen enrichment up to 45% on Jet A1 spray combustion in a swirl-stabilized gas turbine combustor. Using different optical diagnostics, the authors found that the particle volume fraction decreased with hydrogen addition up to 25% but increased at higher enrichment due to hydrogen-air pre-ignition near the nozzle and larger droplets sizes.

For alternative fuels, some studies have focused on the characterization of flame properties in SAF/H_2 mixtures [19,20]. More recently, Singh et al. [21] demonstrated the feasibility of operating SAF/Jet-A1 blends with hydrogen enrichment up to 90% in a low-swirl combustor, reporting notable improvements in flame stability and emissions performance. However, the impact of hydrogen addition on particulate formation mechanisms, soot evolution, and gaseous pollutant emissions in SAF-based flames has not yet been comprehensively characterized. Moreover, systematic experimental investigations focusing on low-swirl combustors operating with hydrogen addition in SAF/Jet A1 blends are still scarce.

This study investigates the influence of H_2 addition on particulate formation and pollutant emissions using a dual-fuel low swirl burner previously reported for low-NO_x operation with Jet A1 and H_2 [8]. The burner operates on a HEFA-SAF/Jet A1 (40:60) blend with varying H_2 concentrations systematically from 0 to 15%. In particular, the work examines how H_2 addition affects particle nucleation and growth, with insights derived from particle size analysis and chemiluminescence imaging to reveal the coupling between H_2 chemistry, soot suppression, and flame stability.

2. Experimental system and measurements

2.1. Experimental rig and operating conditions

Experiments were conducted on a laboratory-scale fuel-flexible combustor using SAF/Jet A1 blend and H_2. A 40:60 HEFA-SAF/Jet A1 blend based on volume was selected as a representative intermediate SAF blending condition to ensure stable burner operation and repeatable atomization characteristics throughout the experimental campaign.The setup comprises an air supply plenum, a quartz-glass combustion chamber (100 × 100 mm^2 cross-section, 460 mm height), with optical access, and an open exhaust, shown in Fig. 1a.

The fuel-flexible nozzle with an effective area of 380 mm^2, which enables dual-fuel operation, is employed in this study (Fig. 1b). This particular nozzle has been utilized in previous investigations [8,21].

HEFA-SAF/Jet A1 (40:60) blend is atomized by a prefilming airblast atomizer system. At first, a pressure swirl atomizer with a flow number of 0.74 (i.e., nozzle flow coefficient), creates a hollow-cone spray with an inner half-angle of 60°.

Secondly, most of the spray is impacting a prefilmer and forms a thin film, which is subsequently atomized at the prefilmer lip by high-velocity air flows.

H_2 is injected through 12 holes from the prefilmer into the outer air channel. The nozzle has two main air supplies separated by the prefilmer lip, along with an additional non-swirling axial flow around the atomizer to prevent flashback near the burner exit plane. One of the main supplies delivers non-swirling air, providing the crossflow for hydrogen injectors, whereas the other is swirled through eight tangentially inclined blades with trailing edges oriented at 45° relative to the nozzle axis. The swirl number associated with this secondary air stream is 0.76, as determined from the vane geometry and the corresponding velocity components. The overall swirl number of the burner is relatively low at around 0.1 to obtain lean lifted flames, which are mainly stabilized by the outer recirculation zone. This swirl number is obtained by accounting for the combined axial and angular momentum fluxes from all three air streams. The relatively low global swirl number results from the inclusion of the non-swirling primary and tertiary air streams, which significantly reduce the net angular momentum. Further details of the burner are given in [8].

The combustor operated at a fixed air inlet temperature of 473 K and an air mass flow rate of 25.3 $g{\cdot}s^{-1}$. The relative pressure drop across the fuel nozzle was maintained at 3%. Lean flames are produced in the experiments with a global equivalence ratio of 0.4 referred to HEFA-SAF/Jet A1 operation. H_2 is blended in the range of 0 to 15% based on thermal power, defined as the ratio of the H_2 thermal contribution to the total thermal power of the HEFA-SAF/Jet A1 and H_2 mixture. Thermal power (P) is calculated as:

$$P = \dot{m}_{H_2} Q_{H_2} + \dot{m}_f Q_f \quad (1)$$

where $\dot{m}_{H_2}$ and $\dot{m}_f$ are the mass flow rates of hydrogen and liquid fuel, respectively, while $Q_{H_2}$and Q_f are their corresponding lower heating values.

The thermal power was kept constant across all experiments to ensure a constant overall energy input, enabling a direct comparison of flame behavior and emissions from dual-fuel combustion. The operating conditions are detailed in Table 1.

2.2. Measurement techniques

Side-view OH* chemiluminescence images were captured with a high-speed camera (Phantom V1212) coupled with an HS-IRO intensifier using a 300–340 nm band-pass filter. A 100 mm UV lens (Cerco) was employed for imaging. The camera acquiring images at 1 kHz over a 5 s interval, capturing images at a resolution of 1280 × 800 pixels.

Exhaust gases were sampled through a heated probe located 440 mm

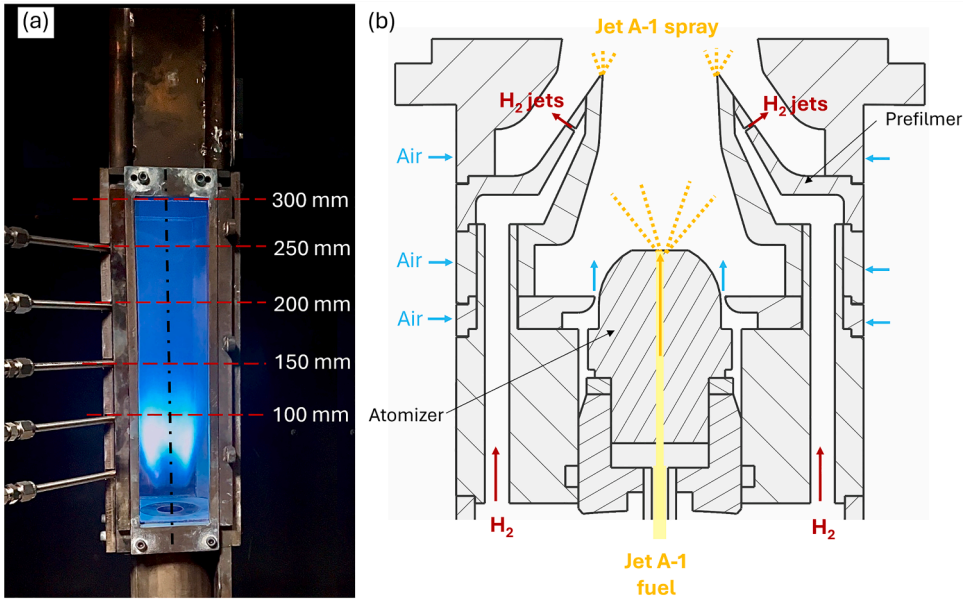


Fig. 1. (a) Fuel-flexible low-swirl combustor with marked sampling probe locations; black dashed line marks the center; red dashed lines indicate axial positions. (b) Schematic view of the fuel nozzle used in this study.

Table 1
Operating conditions in this study.

#OC	H_2%	$\dot{m}_{HEFA/Jet\ A1}$ ($g{\cdot}s^{-1}$)	$\dot{m}_{H_2}$ ($g{\cdot}s^{-1}$)	P (kW)
1	0	0.69	0	31.0
2	2.5	0.67	0.006	31.0
3	7.5	0.64	0.019	31.0
4	15	0.59	0.039	31.0

downstream of the nozzle. The exhaust gases were passed through a dehydrator before being delivered to the analyzers under controlled pressure. The concentrations of O_2 were determined with an ABB Magnos 206 sensor, and concentrations of CO and CO_2 were measured using an ABB Uras 26 analyzer. NO_x was acquired using an Eco Physics CLD 700 EL detector.

Size characterization of aerosol was performed at the reactor outlet and at different heights above the burner nozzle using a Scanning Mobility Particle Sizer (SMPS) with a Nano-DMA (TSI 3085), classifying particles with mobility diameters of 2 – 65 nm. Each scan lasted 30 s, followed by a 12 s purge.

Particle sampling was performed using a vertically oriented stainless-steel probe (10 mm $\varnothing_{outer}$) with a 0.6 mm sampling orifice. The probe had a double-tube design: the outer tube contained the orifice, and the inner concentric tube (6 mm $\varnothing_{outer}$) supplied nitrogen dilution gas at 10 $L{\cdot}min^{-1}$, achieving a 1:40 dilution ratio. Room-temperature nitrogen dilution was used to rapidly quench post-sampling reactions and minimize particle evolution during transport. The selected dilution ratio was chosen to further reduce the already low particle volume fractions and thereby limit post-sampling coagulation, without shifting the particle signal unnecessarily close to the SMPS detection limit.

The probe was inserted into the burner via an automated translation stage. Although intrusive sampling may locally perturb the flow field, no visible modification of flame stability or global flame structure was observed during probe insertion. Measurements were conducted along the height above the nozzle axis at 50 mm intervals from 100 to 300 mm (Fig. 1) and radially at 5 mm intervals, from 5 mm from the centerline up to 30 mm.

3. Experimental results and discussion

3.1. OH* chemiluminescence images

Fig. 2 shows normalized time-averaged OH* chemiluminescence image of HEFA-SAF/Jet A1 flame (OC1–4, Table 1) for various H_2 contents. During the pure HEFA-SAF/Jet A1 operation (Fig. 2a), the high-luminosity heat release zone spans a broad region downstream of the burner exit, characteristic of a lifted spray flame. When H_2 is added (Fig. 2b-d), the heat release region exhibits a slight radial broadening with increasing H_2 content, covering a slightly larger area compared to the pure HEFA-SAF/Jet A1 flame. The lift-off height remains approximately constant around 32.6 mm from the burner exit plane for all fuel blending up to 15% H_2. Overall, the flame structure shows no significant changes, although local temperature variations may occur due to hydrogen-enhanced reaction rates and modified mixing characteristics. likely due to the relatively low radial penetration of the H_2 jet under all operating conditions.

3.2. Pollutant emissions

CO and NO_x emissions, in ppm normalized by 15% O_2 (dry), were measured for varying H_2 content up to 15%. The results show that H_2 addition does have a major impact on CO emission (Fig. 3a), as CO decreases at larger H_2 percentages, but does not affect NO_x emissions (Fig. 3b). The error bars correspond to the standard deviation of the measurements.

The decrease in CO emissions with the addition of small H_2 fractions is well documented in literature. This behavior is generally attributed to hydrogen chemistry, which enhances global combustion kinetics and promotes faster CO oxidation [12,16,18,22]. Although direct comparisons are limited by differences in combustor configuration and operating conditions, comparable trends have been reported in other studies, with CO emissions decreasing by a factor of 1.5 to 5 when up to 15% H_2 is added, in reasonable agreement with the values observed in the present work [16,18].

This work clearly shows that NO_x emission is not significantly affected by H_2 addition. However, effects on NO_x formation remain less clear in the available literature, and flame temperature and equivalence ratio are generally considered more influential parameters for NO_x

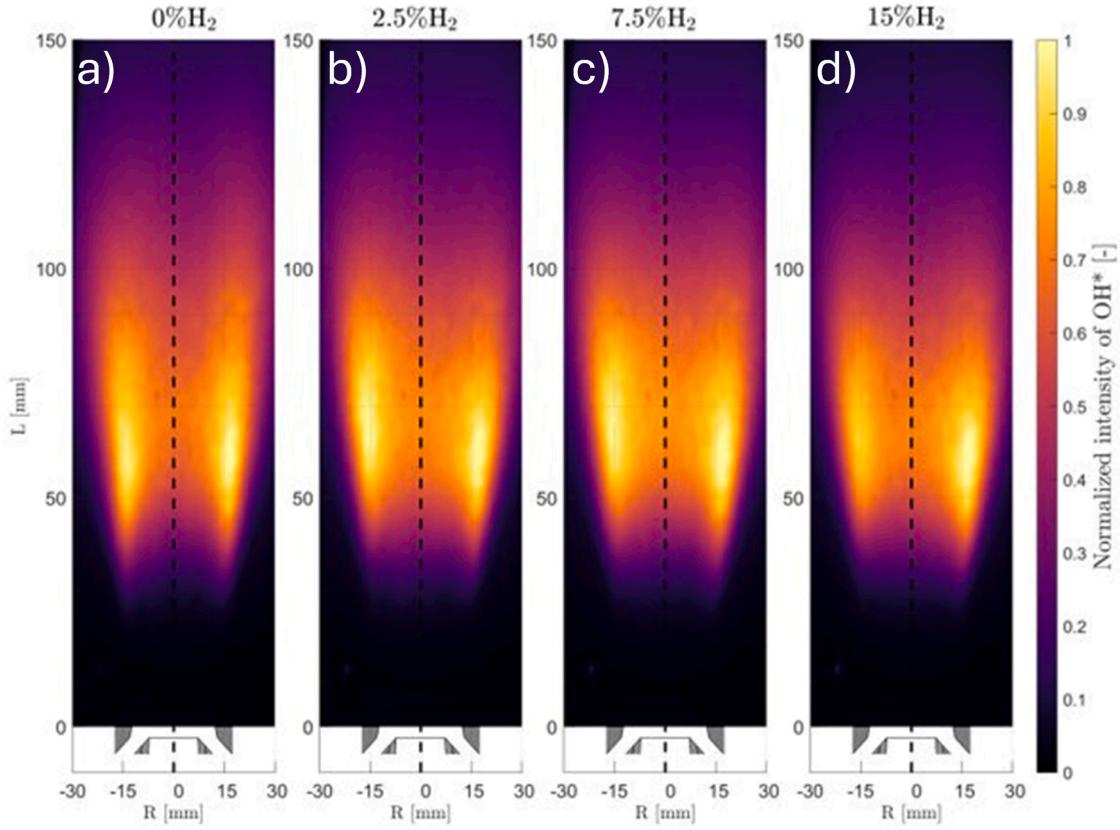


Fig. 2. Normalized time-averaged OH* chemiluminescence image of HEFA-SAF/Jet A1 flame at various H_2 percentages under the operating condition listed in Table 1.

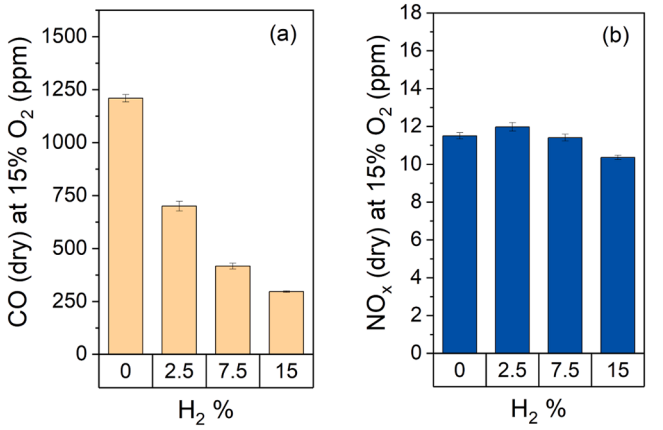


Fig. 3. CO (a) and NO_x (b) emissions at different H_2 percentages conditions (listed in Table 1).

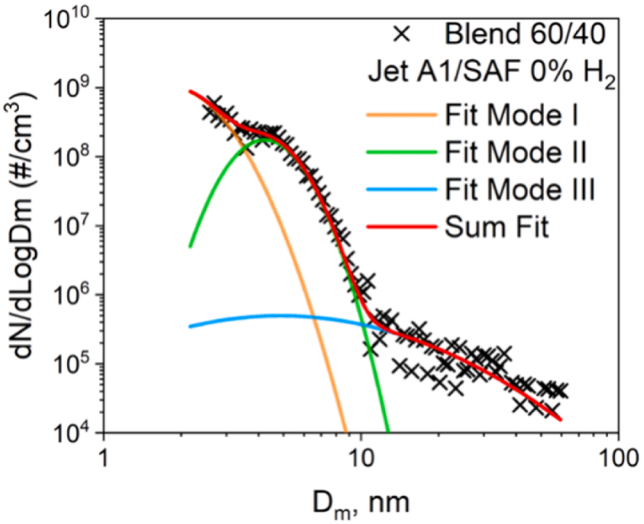


Fig. 4. Particle size distribution (PSDs) for HEFA-SAF/Jet A1 (40/60) flame with 0% H_2, measured at 200 mm from the nozzle and 20 mm from the combustor centerline (see Fig. 1a). Crossed symbols: experimental data; coloured curves: log-normal fits (orange: MC, green: ISP, blue: SP).

emissions than H_2 injection [16].

3.3. Particle size distribution measurements

A typical particle size distribution (PSD) of number concentration measured in the main combustion region is shown in Fig. 4, exhibiting a multimodal shape.

Measurements are corrected for dilution and diffusive losses in the transport line from the probe orifice to the instrument inlet and provide particle size distributions and number concentrations at various combustor locations. They exhibit a multimodal shape, with particle sizes ranging from 2 to approximately 65 nm. Size distributions have been deconvoluted into three log-normal distributions having mean sizes at 2.0, 4.5, and 12 nm with geometric standard deviations of 1.35, 1.28, and 2.23, respectively. These values have been typically used to fit the particle size distributions measured in flames [23]. The fitting procedure was performed using constrained modal diameters based on previous experimental studies in similar combustion systems. Sensitivity tests were performed by perturbing the initial fitting parameters and by

varying the fitting constraints adopted for the three log-normal modes. Although small variations in modal position and relative amplitude were observed, the overall identification of the three particle classes and the main trends with H_2 addition remained robust within the uncertainty of the deconvolution procedure. Alternative reasonable fits did not lead to different physical interpretations.

Based on previous laboratory measurements, we attribute the three modes to Molecular Clusters – MC – (2 nm mode), to Incipient Soot Particles – ISP – (4.5 nm mode), and finally to Soot Particles – SP – (12 nm mode) (see Fig. 8 in [24]).

Mode I MCs, orange curve in Fig. 4, primarily consists of clusters of high-molecular mass polycyclic aromatic hydrocarbon (PAH) molecules stabilized by weak van der Waals forces. These compounds are probably formed during the combustion process or derive from the residue high molecular mass hydrocarbons of the fuel blend. Mode II ISPs, green curve, originates from the coagulation of smaller precursors and growth by surface reactions, with the process potentially enhanced by covalent-like bonding among Mode I particles that promote the formation of a three-dimensional network. Finally, Mode III SPs, blue curve, arise from further growth of smaller aggregates, yielding particles larger than 10 nm in diameter. Using the same fitting parameters, all PSDs measured under different flame conditions were analysed. Distinct trends in all three modes were observed along both the radial and axial directions, offering detailed insight into particle evolution within the combustor.

Fig. 5 shows the radial evolution of total particle number concentration measured 200 mm downstream of the burner at 0% H_2. Along the radial direction (5 mm radial position is near the centreline of the combustion chamber and 30 mm is near the combustor wall), the total particle number concentration N_{tot} exhibits a clear decreasing trend. In the center of the combustor chamber, N_{tot} remains relatively high, around $3.5{\cdot}10^8$ #/cm^3, and subsequently decreases sharply toward the burner wall, reaching approximately $5.0{\cdot}10^7$ #/cm^3 at 30 mm.

The data indicate a predominant contribution from MC, which follows the same trend as the total number concentration, particularly near the centre of the combustion chamber. Moving radially outward, the contribution of MC progressively decreases, while ISPs start forming, reaching the maximum number concentration between 20 and 25 mm in correspondence with the maximum intensity of the flame (see Fig. 2). Notably, SPs are not detected in this burner location.

From the number concentration profiles, it is possible to calculate the particle volume fractions, shown in Fig. 6, of the detected particles under the hypothesis of spherical shape. The volume fraction

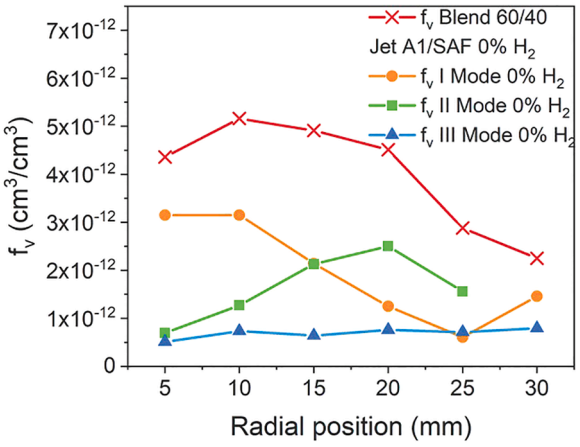


Fig. 6. Particle volume fraction versus radius for HEFA-SAF/Jet A1(40/60) flame with 0% H_2, measured at 200 mm from the nozzle (see Fig. 1a), showing total fraction and contributions of Mode I (orange circles), Mode II (green squares), and Mode III (blue upward triangles).

determined by SMPS is very low, of the order of 10^{-11} cm^3·cm^{-3}, showing also a non-sooting tendency of the burner configuration. MCs are the predominant species formed close to the burner axis, whereas ISPs are formed across the spray region but in a very low concentration.

Next, the effect of H_2 addition on soot formation is evaluated. Fig. 7 shows the PSDs as a function of the mobility diameter (D_m) for different H_2 concentrations (as described in Table 1) measured at 200 mm from the combustion chamber exit and 20 mm from the combustor centerline.

All distributions exhibit the number concentration trend decreasing monotonically as the particle diameter increases. However, the addition of 2.5% H_2, is associated with a slight increase in the number of particles, particularly in the 2–3 nm diameter range, which may suggest a tendency toward enhanced formation of early aromatic precursors, although larger uncertainty is associated with these ultrafine particles. Further increases in H_2 concentration progressively reduce the particle number concentration, consistent with an overall suppression of particle formation at higher H_2 blends.

The total particle number concentration (N_{tot}) exhibits a variable behaviour. Measurements at different H_2 concentrations were taken at

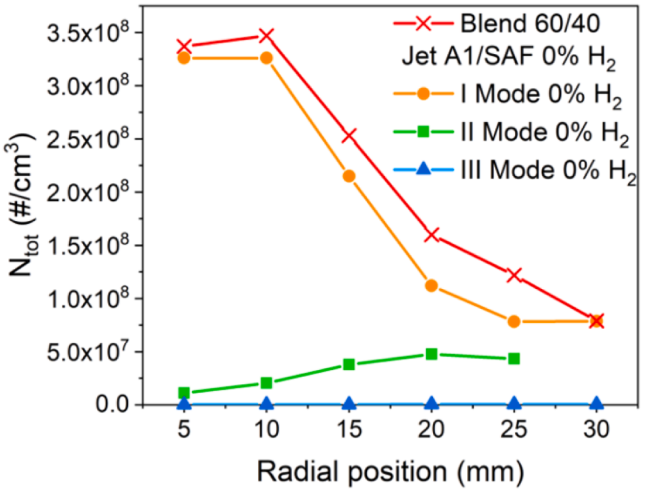


Fig. 5. Particle number concentration versus radial position for HEFA-SAF/Jet A1(40/60) flame with 0% H_2, measured at 200 mm from the nozzle (see Fig. 1a), showing total concentration and contributions of the three modes: Mode I (orange circles), Mode II (green squares), and Mode III (blue triangles).

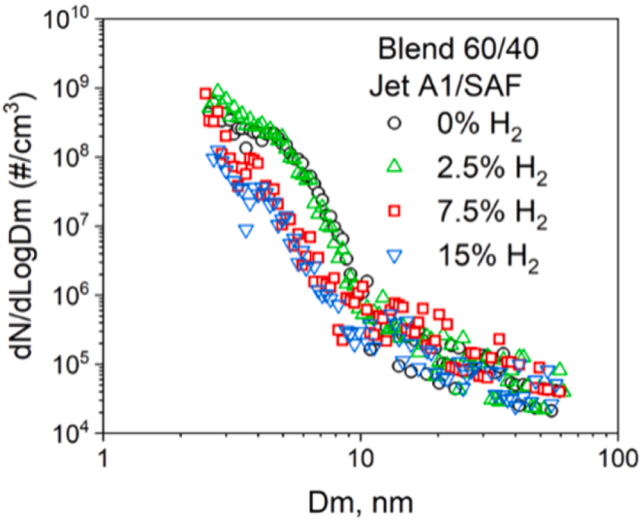


Fig. 7. Particle size distributions (PSDs) measured at 200 mm downstream and 20 mm radial distance from the combustor center, as a function of H_2 addition (see Fig. 1a). Symbols: black circles – 0% H_2, green upward triangles – 2.5% H_2, red squares – 7.5% H_2, blue downward triangles – 15% H_2.

selected sampling heights. At a height of 100 mm above the burner exit, the total number concentration progressively decreases with increasing H_2 content, starting from a value of about $5{\cdot}10^8$ at 0% H_2 to $3{\cdot}10^8$ at 15% of H_2. At 200 mm from the burner exit, corresponds to the region just above the flame high-luminosity reaction zone, the situation appears notably different: the number of particles generated with the addition of 2.5% H_2 is significantly higher, i.e., from $1.5{\cdot}10^8$ to $3{\cdot}10^8$, followed by a decrease at 250 mm, where the values were about $1{\cdot}10^8$. In contrast, for the 7.5% and 15% H_2 cases, the particle number concentration remains consistently lower at all investigated heights, at about $5{\cdot}10^7$.

To further understand this effect, the particle volume fraction was compared at different heights and hydrogen blends. In Fig. 8, the particle volume fraction (f_v) evaluated at 20 mm in the radial position from the combustor centerline is plotted against the distance from the nozzle at different H_2%. In this position from the centerline axis, maximum f_v values are reported under the 0% H_2. Globally, increasing the H_2 concentration leads to progressively lower particle volume fractions, with the effect becoming more pronounced at larger axial distances from the nozzle.

However, at 200 mm, the addition of 2.5% H_2 does not produce a local decrease in particle volume fraction compared to higher H_2 concentrations. Although probe dilution, particle deposition within the sampling line, diffusion losses, probe heating, and probe positioning may introduce non-negligible uncertainties, the observed tendency was qualitatively reproducible across repeated measurements and remained consistent with the independently measured particle number concentration trends.

To further examine the effect of small H_2 addition, Fig. 9 shows particulate conversion ratio (C_s) normalized by C_s at 0% H_2, against the H_2 admixture at different positions in the burner. Following [10], C_s can be defined as:

$$C_s = \frac{S{\cdot}\dot{m}_a}{\dot{m}_f{\cdot}(1 - R_h)} \tag{2}$$

where S is particulate concentration (in this work particulate volume fraction, f_v, was used), $\dot{m}_a$ and $\dot{m}_f$ are air and fuel flow rates, respectively, and R_h is H_2 percentage. This conversion ratio represents an index of the changing degree of HEFA-SAF/Jet A1 blend to carbonaceous particulate.

Fig. 9 shows that the particulate conversion ratio C_s decreases by a factor of approximately 3 to 8 when increasing the hydrogen content from 0 to 15% H_2 blend, relative to the baseline condition. Error bars

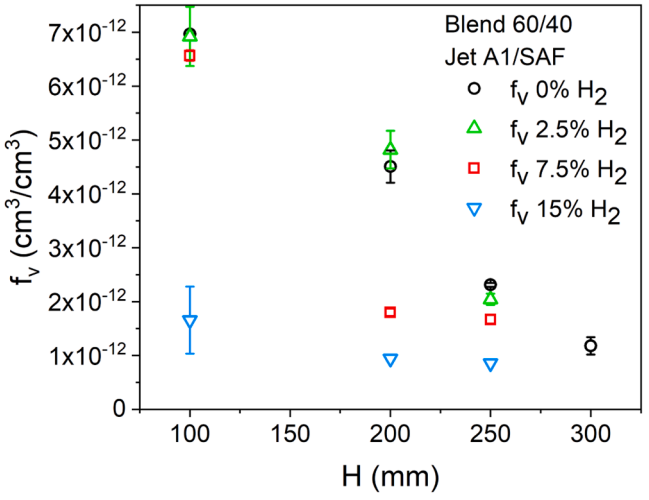


Fig. 8. Particle volume fraction (f_v) at 20 mm from the centerline of the combustor along the axial direction (see Fig. 1a). Markers: black circles – 0% H_2, green upward triangles – 2.5% H_2, red squares – 7.5% H_2, blue downward triangles – 15% H_2.

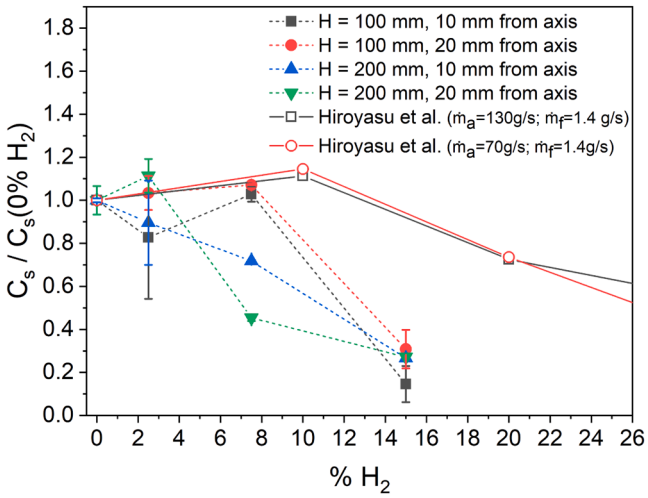


Fig. 9. Particulate conversion ratio (C_s) normalized on C_s at 0% H_2. The reported error bars are related to standard deviations of repeated measurements.

express, whenever possible, standard deviations calculated from repeated measurements. At 100 mm from the nozzle, the effect of H_2 addition on particulate suppression becomes relevant only at the 15% H_2 blend. At 2.5% H_2 and 10 mm from the centerline, a slight reduction is observed, although associated with large uncertainty, while no significant variation is detected at 20 mm. At the 7.5% H_2 blend, the particulate conversion ratio increases again to values comparable to, or slightly larger than, those measured for the 0% H_2 blend. At 200 mm from the nozzle and for 2.5% H_2 blend a slight decrease in particulate conversion ratio is observed at 10 mm from centerline, despite a clear trend cannot be identified due to significant uncertainty, while a slight increase appears at 20 mm for the same condition. In both cases (10 mm and 20 mm), at 7.5% H_2 a reduction in particulate volume fraction is noticed. These results suggest that small H_2 fractions in the fuel mixture (i.e., 2.5%) do not suppress particle formation; in some cases, they may even increase the formation of early particulate precursors.

At low H_2 addition levels, multiple competing effects may coexist. On the one hand, hydrogen-enhanced radical chemistry and local mixing effects, facilitated by the high diffusivity of H_2 may promote the formation of aromatic precursors and early particle nucleation [25,26]. On the other hand, increasing hydrogen content progressively reduces the carbon available for soot formation and enhances oxidation pathways, ultimately suppressing particle growth. The present results suggest that, at very low H_2 addition (2.5%), these promoting effects may still locally compensate for the soot-suppression mechanisms. At higher H_2 fractions, however, the suppressing effects become dominant, leading to a monotonic reduction in particulate formation.

At higher H_2 blends, the influence of enhanced radical chemistry no longer outweighs the effect of carbon depletion, as observed at 15% H_2 blends. At this level, H_2 addition generally suppresses both the total particle number and the overall particulate volume fraction, which, according to the present results, is reduced by a factor of 4 to 6 relative to the 0% H_2 case (Fig. 8). This confirms the expected inhibition on particle growth and coagulation.

Fig. 9 presents a rough comparison between data adapted from Hiroyasu et al. [12] and the results of the present study. Hiroyasu et al. [12] reported an increase in the particulate conversion ratio for H_2 blending up to 10%. On the other hand, a thorough quantitative comparison is not possible, as different burner configurations and operating conditions were considered, and soot concentration was evaluated through a different procedure.

Overall, higher H_2 blending levels strongly suppressed soot nucleation and growth, achieving flames with near-zero particulate emissions. These findings confirm a strong inhibiting effect of H_2 on particle

growth and coagulation mechanisms, even though this effect appears less pronounced (or absent) at low H_2 contents.

4. Conclusion

This study investigated the influence of hydrogen addition on particulate formation in a dual-fuel low-swirl combustor operating with a HEFA-SAF/Jet A1 (40:60) blend. The burner configuration, previously demonstrated to achieve very low NO_x emissions during Jet A1/H_2 operation, also showed a strong capability to limit particulate formation under the investigated conditions.

The results indicate that hydrogen addition significantly affects particle formation dynamics. Increasing the H_2 fraction in the fuel mixture progressively suppresses particle formation, ultimately leading to near-zero particulate emissions at the highest investigated hydrogen content. However, this reduction becomes pronounced only at sufficiently high H_2 concentrations.

At low H_2 addition (2.5%), a slight increase in particle formation was observed. This behaviour is likely related to local variations of mixture composition due to high hydrogen diffusivity, and kinetic effects associated with hydrogen chemistry. The enhanced availability of reactive H radicals can promote the formation of aromatic species and polycyclic aromatic hydrocarbons (PAHs), thus facilitating the early stages of particle nucleation.

At higher H_2 fractions, the reduction in carbon availability combined with modified reaction pathways becomes dominant, leading to a strong suppression of particle nucleation and growth. These findings highlight the complex role of hydrogen in particulate formation processes and demonstrate that sufficiently high hydrogen blending levels can effectively mitigate soot formation in SAF/Jet A1 spray flames.

These findings highlight the complex role of hydrogen in particulate formation processes and demonstrate that sufficiently high hydrogen blending levels can effectively mitigate soot formation in SAF/Jet A1 spray flames. Overall, the present results support the potential of hydrogen-assisted combustion for reducing particulate emissions under the investigated lean low-swirl operating conditions. Further investigations under more engine-relevant conditions are required to assess the broader applicability of the observed trends to future sustainable aviation propulsion systems.

Declaration of competing interest

The authors declare that they have no known competing financial interests or personal relationships that could have appeared to influence the work reported in this paper.

Acknowledgements

The research leading to these results has received funding from the European Union (Project: FFLECS; Grant agreement ID 101096436). Views and opinions expressed are however those of the authors only and do not necessarily reflect those of the European Union. Neither the European Union nor the granting authority can be held responsible for them.

References

[1] D.S. Lee, D.W. Fahey, A. Skowron, M.R. Allen, U. Burkhardt, Q. Chen, S.J. Doherty, S. Freeman, P.M. Forster, J. Fuglestvedt, A. Gettelman, R.R. De León, L.L. Lim, M. T. Lund, R.J. Millar, B. Owen, J.E. Penner, G. Pitari, M.J. Prather, R. Sausen, L. J. Wilcox, The contribution of global aviation to anthropogenic climate forcing for 2000 to 2018, Atmos. Environ. 244 (2021) 117834.
[2] I. Abrantes, A.F. Ferreira, A. Silva, M. Costa, Sustainable aviation fuels and imminent technologies - CO2 emissions evolution towards 2050, J. Clean. Prod. 313 (2021) 127937.
[3] B. Wang, Z.J. Ting, M. Zhao, Sustainable aviation fuels: key opportunities and challenges in lowering carbon emissions for aviation industry, Carbon Capture Sci. Technol. 13 (2024) 100263.
[4] F. Yang, Y. Yao, Sustainable aviation fuel pathways: emissions, costs and uncertainty, Resour. Conserv. Recycl. 215 (2025) 108124.
[5] A. Gomez, H. Smith, Liquid hydrogen fuel tanks for commercial aviation: structural sizing and stress analysis, Aerosp. Sci. Technol. 95 (2019) 105438.
[6] Y.S.H. Najjar, Hydrogen safety: the road toward green technology, Int. J. Hydrogen. Energy 38 (2013) 10716–10728.
[7] P. Agarwal, X. Sun, P.Q. Gauthier, V. Sethi, Injector design space exploration for an ultra-low NOx hydrogen micromix combustion system, in: Proceedings of the ASME Turbo Expo, American Society of Mechanical Engineers (ASME), 2019 GT2019-90833.
[8] S. Singh, M. Amerighi, N. Scopolini, A. Andreini, S.R. Harth, D. Trimis, Effect of H2 and Jet-A1 fuel split on flame stability and pollutant emissions from low-swirl burner, Proc. Combust. Inst. 41 (2025) 105858.
[9] K. Kikuchi, T. Hori, F. Akamatsu, Fundamental study on hydrogen low-NOx combustion using exhaust gas self-recirculation, Processes 10 (2022) 130.
[10] E.J. Adler, J.R.R.A. Martins, Hydrogen-powered aircraft: fundamental concepts, key technologies, and environmental impacts, Prog. Aerosp. Sci. 141 (2023) 100922.
[11] S. Manigandan, T.R. Praveenkumar, J. Ir Ryu, T.N. Verma, A. Pugazhendhi, Role of hydrogen on aviation sector: a review on hydrogen storage, fuel flexibility, flame stability, and emissions reduction on gas turbines engines, Fuel 352 (2023) 129064.
[12] H. Hiroyasu, M. Arai, T. Kadota, J. Yoso, An experimental study on kerosene-hydrogen hybrid combustion in a gas turbine combustor, Bull. JSME 23 (1980) 1655–1662.
[13] K. Dave, S. Link, F. De Domenico, F. Schrijer, F. Scarano, A. Gangoli Rao, Kerosene-H2 blending effects on flame properties in a multi-fuel combustor, Fuel Commun. 23 (2025) 100139.
[14] L. Miniero, K. Pandey, G. De Falco, A. D'Anna, N. Noiray, Soot-free and low-NO combustion of Jet A-1 in a lean azimuthal flame (LEAF) combustor with hydrogen injection, Proc. Combust. Inst. 39 (2023) 4309–4318.
[15] J. Burguburu, G. Cabot, B. Renou, A.M. Boukhalfa, M. Cazalens, Effects of H2 enrichment on flame stability and pollutant emissions for a kerosene/air swirled flame with an aeronautical fuel injector, Proc. Combust. Inst. 33 (2011) 2927–2935.
[16] J.P. Frenillot, G. Cabot, M. Cazalens, B. Renou, M.A. Boukhalfa, Impact of H2 addition on flame stability and pollutant emissions for an atmospheric kerosene/air swirled flame of laboratory scaled gas turbine, Int. J. Hydrogen. Energy. 34 (2009) 3930–3944.
[17] G.L. Juste, Hydrogen injection as additional fuel in gas turbine combustor. Evaluation of effects, Int. J. Hydrogen. Energy. 31 (2006) 2112–2121.
[18] S. Mohammadnejad, A. Azimi, R.K. Maurya, Ö.L. Gülder, Influence of premixed hydrogen enrichment on Jet A-1 spray combustion in a swirl-stabilized model gas turbine combustor, Combust. Flame 286 (2026) 114847.
[19] C. Hong, J. Subburaj, J. Zou, A.M. Elbaz, W.L. Roberts, Z. Huang, Y. Zhang, A. Farooq, Laminar flame speed of hydrogen-enriched sustainable aviation fuel: experiments and chemical kinetic modeling, Combust. Flame 283 (2026) 114613.
[20] M.Z. Akram, Study of hydrogen impact on lean flammability limit and burning characteristics of a kerosene surrogate, Energy 231 (2021) 120925.
[21] S. Singh, F.P. Hagen, S. Harth, D. Trimis, Comparative Study of Hydrogen Addition Effects on Flame Stability and Pollutant Emissions in Jet-A1 and Sustainable Aviation Fuel/Jet-A1 Lean Lifted Spray Flames, J. Eng. Gas Turbines Power 148 (12) (2026) 121009.
[22] S. Tamang, H. Park, An investigation on the thermal emission of hydrogen enrichment fuel in a gas turbine combustor, Int. J. Hydrogen. Energy. 48 (2023) 40071–40087.
[23] C. Liu, A.V. Singh, C. Saggese, Q. Tang, D. Chen, K. Wan, M. Vinciguerra, M. Commodo, G. De Falco, P. Minutolo, A. D'Anna, H. Wang, Flame-formed carbon nanoparticles exhibit quantum dot behaviors, Proc. Natl. Acad. Sci. USA 116 (2019) 12692–12697.
[24] G. Vitiello, G. De Falco, F. Picca, M. Commodo, G. D'Errico, P. Minutolo, A. D'Anna, Role of radicals in carbon clustering and soot inception: a combined EPR and Raman spectroscopic study, Combust. Flame 205 (2019) 286–294.
[25] M. Wang, X. Qian, Y. Suo, Y. Ye, G. Li, Z. Zhang, Effect of hydrogen addition on soot formation and emission in acetylene laminar diffusion flame, ACS. Omega 8 (2023) 24893–24900.
[26] M. Frenklach, Reaction mechanism of soot formation in flames, Phys. Chem. Chem. Phys. 4 (11) (2002) 2028–2037.